X-ray photoemission determination of the Schottky barrier height of metal contacts to *n*–GaN and *p*–GaN

K. A. Rickert and A. B. Ellis
Department of Chemistry, University of Wisconsin-Madison, Madison, Wisconsin 53706

Jong Kyu Kim and Jong-Lam Lee
Department of Materials Science and Engineering, Pohang University of Science and Technology, Pohang, Korea

F. J. Himpsel
Department of Physics, University of Wisconsin-Madison, Madison, Wisconsin 53706

F. Dwikusuma and T. F. Kuech[a)]
Department of Chemical Engineering, University of Wisconsin-Madison, Madison, Wisconsin 53706

(Received 1 July 2002; accepted 10 September 2002)

Synchrotron radiation-based x-ray photoemission spectroscopy was used to study the surface Fermi level position within the band gap for thin metal overlayers of Au, Al, Ni, Ti, Pt, and Pd on *n*–GaN and *p*–GaN. Nonequilibrium effects were taken into account by measuring the Fermi edge of the metal overlayer. There are two different behaviors observed for the six metals studied. For Au, Ti, and Pt, the surface Fermi level lies about 0.5-eV higher in the gap for *n*-type than for *p*-type GaN. For Ni, Al, and Pd, the surface Fermi level position is independent of doping, but varies from one metal to the other. Results for Ni, Pd, and Al fit a modified Schottky–Mott theory, while Au, Ti, and Pt demonstrate a more complex behavior. Atomic force microscopy was used along with photoemission to investigate the growth mode of each metal on the GaN surface. © *2002 American Institute of Physics.* [DOI: 10.1063/1.1518129]

INTRODUCTION

The development of high-quality GaN growth techniques has opened many device applications. GaN has a direct band gap of 3.4 eV, which leads to shorter wavelength light emission that is used in a variety of optical applications, including light emitting diodes[1] and laser diodes. GaN also has advantages in high-power devices.[2]

The large band gap of GaN makes the formation of low-resistance ohmic contacts more difficult than for many other III-V semiconductors. Contacts to *p*-type GaN have been particularly challenging, since it is difficult to grow samples with a high enough carrier concentration to promote field emission through the Schottky barrier. Due to the complexity of metallurgical contacts, various approaches have been tried, including chemical surface treatments,[3–7] plasma cleaning,[8–10] metal deposition techniques (sputtering, electron beam, or thermal deposition),[11–13] contact annealing in a variety of ambients,[14,15] and use of bilayers[16–18] or multilayers[19–21] of various metals.

Most previous studies have focused on the electronic properties of a single metal on either *n*–GaN or *p*–GaN surfaces. Results from these studies are difficult to compare directly due to the differences in sample carrier concentration, surface preparation prior to deposition, and in the techniques used to characterize the contact electronic properties (current-voltage, capacitance-voltage, and internal photoemission). In this investigation, a systematic study comparing six metals on identically prepared samples was carried out, allowing a direct comparison of the surface electronic properties. The object in studying single metals is to determine what parameters, if any, of the metal affect the electronic properties of the contact.

Previously, we have reported on the effects of HCl and KOH treatments on both *n*–GaN and *p*–GaN.[3,4] The effect of these treatments on the surface chemistry was correlated with the electronic properties through monitoring changes in the movement of the Ga 3*d* core level. The KOH treatments led to a decreased Ga/N ratio on the surface for both *n*– and *p*–GaN. On *p*–GaN, KOH treatment leads to a decrease in band bending and therefore to a reduction of the surface-barrier height. On *n*–GaN, HCl treatment led to a higher Ga/N ratio relative to the untreated surface and to a decrease in band bending and surface-barrier height. The contact resistance (ρ_c) is determined by the surface-barrier height Φ_B through

$$\rho_c = \frac{k_B}{qA^*T}\exp\left[\frac{q\Phi_B}{k_BT}\right], \tag{1}$$

where k_B is Boltzmann's constant, q is the electron charge, A^* is the effective Richardson's constant, and T is temperature (Kelvin). A small reduction in the surface-barrier height will have a large effect in reducing the contact resistance in Schottky barrier-based contacts.

Synchrotron-based x-ray photoemission spectroscopy can be used to investigate the surface electrical properties during metal deposition on GaN samples. A photon energy is chosen for a specific core level to minimize the electron es-

a)Electronic mail: kuech@engr.wisc.edu

cape depth, which results in an enhanced surface sensitivity.[22] The metal forming the contact is deposited *in situ* within an ultrahigh vacuum chamber, and the measurements can be made as a function of metal coverage. The direct measurement of the surface-barrier height avoids complications and assumptions associated with other measurements. For example, defects at the semiconductor-metal interface can lead to complications in current-voltage (I-V) measurements of the surface-barrier height.[23] Capacitance-voltage (CV) determinations of the barrier height can also be complicated by these defects, which alter the space-charge region and affect the measured flat band voltage.[23] The surface-barrier height for p–GaN, $\Phi_{B,p}$, can be determined from the binding energy of a given core level E_B and the energy difference between that core level and the valence-band maximum $E_{V\text{-}C}$ according to Eq. (2), as reviewed in a recent article by Tung.[24]

$$\Phi_{B,p} = |E_B| - E_{V-C} \tag{2}$$

EXPERIMENT

The n–GaN samples were grown using metal-organic vapor phase epitaxy (MOVPE), on c-plane sapphire with a 20-nm GaN buffer layer followed by 1.3 μm of Si-doped n–GaN. The carrier concentration at the sample surface is $4-7\times10^{18}$ cm^{-3}, as determined by capacitance-voltage measurements. The samples were treated with HCl:H_2O, 1:2 by volume, for 2 min. The samples were mechanically masked and then 150-nm-thick Ti patches were deposited on the edges with an electron-beam evaporator to provide electrical contacts. Finally, the samples were annealed in ultrahigh-purity Ar at 800 °C for 30 sec.

The p–GaN samples were grown by MOVPE on c-plane sapphire substrates. An undoped GaN layer with a thickness of 1 μm was grown, followed by the growth of 3-μm-thick p-type GaN doped with Mg. The GaN:Mg samples were annealed at 800 °C for 4 min by rapid thermal annealing (RTA) under a N_2 atmosphere to activate the Mg acceptors. The net concentration of holes in the film was 3.3×10^{17} cm^{-3}, and hole mobility was 15.8 cm^2/V s, as determined using room-temperature Hall-effect measurements. Before the deposition of Pt on the p–GaN, which was used to form broad area ohmic contacts, the samples were cleaned using ultrasonic baths in beakers of acetone for 5 min and beakers of isopropyl alcohol for 5 min, followed by a deionized (DI) water rinse for 10 min. Samples were blown dry with N_2, then dipped into boiling aqua regia solution for 10 min. The samples were next rinsed with DI water for 10 min, and then once more blown dry with N_2. Pt ohmic contacts were subsequently deposited with a thickness of 300 nm, using electron-beam evaporation under a vacuum of less than 5×10^{-7} Torr.

The photoemission experiments were done on the Mark II and 6 M TGM beamlines at the University of Wisconsin-Madison Synchrotron Radiation Center in an ultrahigh vacuum chamber equipped with a Cylindrical Mirror Analyzer (CMA). After the deposition of ohmic contact patches described above, the samples were loaded into the chamber and photoemission data for the sample without metal was initially acquired as well as data for increasing metal coverage. This process continued until the metal overlayer became thick enough so that the underlying Ga 3d core-level peak could no longer be detected. This procedure was carried out in turn with Au, Ti, Ni, Pt, Pd, and Al on identically prepared substrates of both n–GaN and p–GaN. The spectrometer was calibrated using a clean Ta foil to determine the conversion from the measured kinetic energy to the binding energy via the effective spectrometer work function.

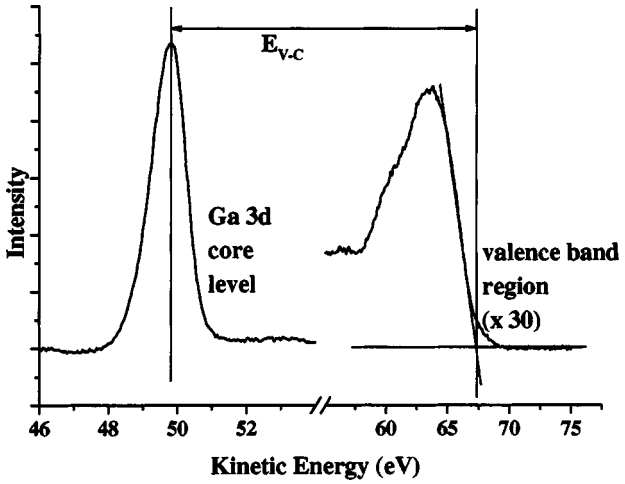

FIG. 1. The left-hand spectrum shows the Ga 3d core-level photoemission peak on n–GaN without a metal overlayer. The right-hand figure presents the spectrum of the valence-band region. A linear fit is used to determine the kinetic energy of the valence-band edge. These two spectra determine the value of $E_{V\text{-}C}$, as indicated by the double arrow.

The binding energy of the Ga 3d core-level E_B is used in the determination of the surface-barrier height at each metal coverage, Eq. (2). This conversion is only possible under equilibrium conditions. In our study, nonequilibrium effects were evident, since the measured Fermi edges on our semiconductor samples were not aligned with the reference Fermi edge of the Ta foil. These effects could be due to a surface photovoltage effect or to a resistive voltage drop at the contacts of the sample and at the depletion region below the surface[25] and are mentioned in Ref. 4. These effects lead to a change in the band bending and can complicate the measurement of the surface-barrier height as previously observed during the investigation of Au deposition on GaN via photoemission.[26,27] The broad area ohmic contacts to GaN reduced such effects but could not eliminate them completely. Nevertheless, the surface Fermi level can be determined even under nonequilibrium conditions.[28] The valence-band and Ga 3d core-level spectra on the surface without metal deposited are used to determine the energy difference between these two levels ($E_{V\text{-}C}$), which is a bulk property of GaN and therefore independent of metal coverage. Figure 1 shows an example of the Ga 3d core-level and the valence-band spectrum collected on an n–GaN sample without a metal overlayer. When metal is deposited on the sample surface, the edge of the valence-band maximum can no longer be seen, since it is obscured by the signal originating from the metal overlayer. The Fermi edge of the metal, which

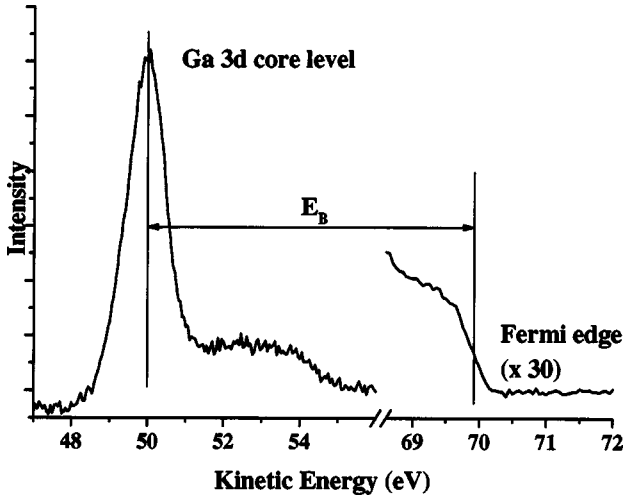

FIG. 2. The left-hand spectrum displays the Ga 3*d* core level of *n*–GaN after the deposition of 0.4 nm of Au on the surface. The right side includes the Fermi edge measured on the same sample. These spectra generate a value of E_B (double arrow) that is free of nonequilibrium effects.

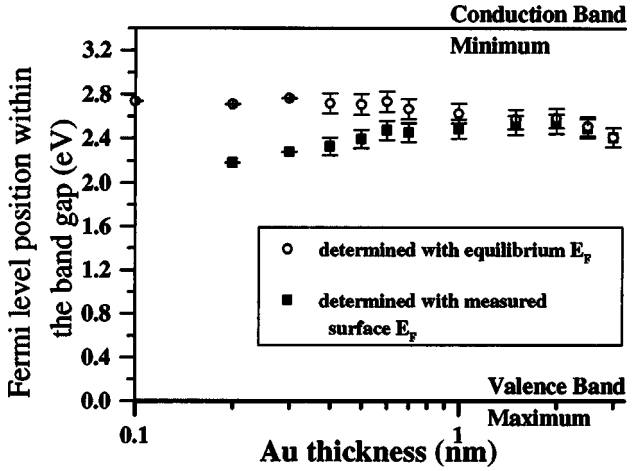

FIG. 3. The position of the Fermi level within the band gap of *n*–GaN is shown with respect to the valence-band maximum. For the squares, the Fermi edge was determined at the sample surface for each coverage of Au, which takes nonequilibrium effects into account. For the circles, a Ta foil was used as a reference for the Fermi edge.

indicates the Fermi level position at the semiconductor surface, can now be observed.

Figure 2 shows the Ga 3*d* core level and the Fermi edge spectra of an *n*–GaN sample with a 0.4-nm Au overlayer. These spectra determine the Ga 3*d* binding energy E_B relative to the Fermi-level E_F. Nonequilibrium effects shift both the Ga 3*d* core level and the Fermi edge by the same amount but the difference in E_B remains unaffected. Since the peak shift changes with coverage, the Au Fermi edge needs to be measured for each coverage to ensure an accurate determination of E_B. The *p*-type surface-barrier height is determined using Eq. (2) by combining E_B at each coverage with $E_{V\text{-}C}$, determined from the surface without metal, as shown in Fig. 1. The Ga 3*d* peaks were fit to a Gaussian function to determine the peak center. The first derivative of the Fermi edges is fit to a Gaussian, as well, and used to determine the Fermi-level energy after each metal deposition.

When the samples were removed from the analysis chamber they were analyzed via tapping mode atomic force microscopy (AFM) in order to determine the surface morphology and the growth mode of the metal on the sample surface.

RESULTS

The effects of chemical treatments on the Fermi level of the bare surface were described in detail in the publications listed as Refs. 3 and 4. The results for the effects of metal deposition on the chemically treated GaN surfaces are described in this work. Figure 3 shows the plot of the Fermi-level position within the band gap with respect to the valence-band maximum for the deposition of Au on *n*–GaN. One set of data, indicated by the circles, represents the position determined with E_B, which was determined with the Ta foil Fermi edge as our reference. The other set of data, indicated by the squares, is from E_B determined with the Au Fermi edge measured on the sample surface directly. This latter set should be considered to be free from the contribution of nonequilibrium effects. The difference between these two sets of data can be related to the magnitude of the nonequilibrium effects and can be seen to decrease with increasing coverage. The results obtained using the Ta foil edge give a different and erroneous surface-barrier height, particularly at low coverages.

To compare the position of the Fermi level on both *n*–GaN and *p*–GaN, the data from the directly measured Au Fermi level after each deposition of Au are shown in Fig. 4. The Au Fermi level position for *n*–GaN is about 0.5-eV higher within the band gap than for *p*–GaN. Similar information is shown for the deposition of Ni on *n*–GaN and *p*-GaN in Fig. 5. Unlike the case of Au, the Ni Fermi level for both *n*–GaN and *p*–GaN appears at the same location within the band gap within experimental error; a preliminary version of these results for Au, Ni, and Ti was reported previously.[29] The same analysis was done for the other three metals, and the summary

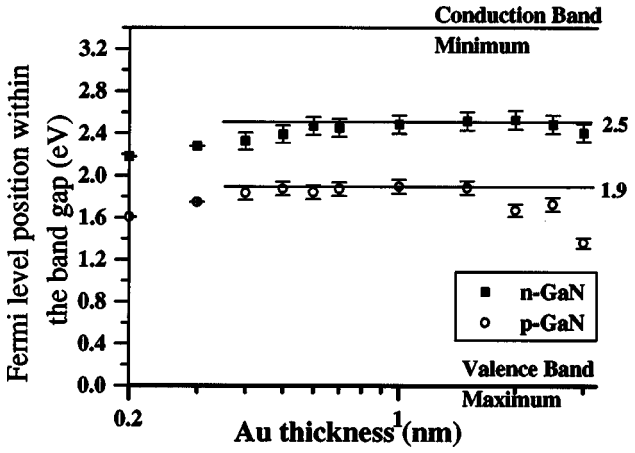

FIG. 4. The position of the Fermi level within the band gap of *n*–GaN and *p*–GaN is shown with respect to the valence-band maximum. The Fermi edge was measured on the sample for each coverage of Au. A separation of 0.5 eV within the gap is seen for the Fermi-level position between *n*–GaN and *p*–GaN.

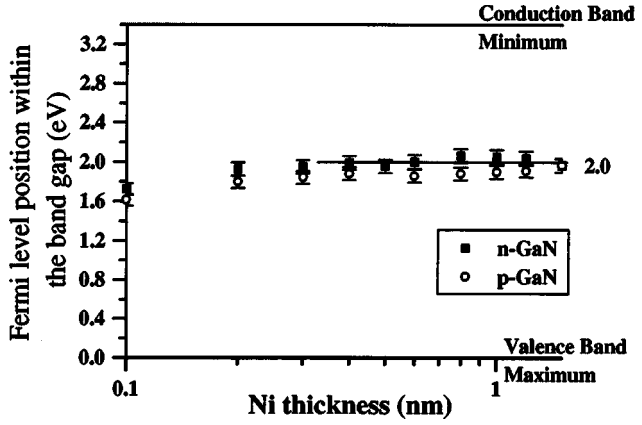

FIG. 5. A plot similar to Fig. 4 is presented for Ni as the metal overlayer.

of results is shown in Fig. 6. For $n(p)-$GaN, Φ_B is equal to the difference between the conduction- (valence-) band minimum and the Fermi-level position within the band gap. The band gap of GaN is taken to be 3.4 eV. The surface-barrier height results are summarized in Table I.

Two types of pinning behavior are observed for the metals in this study. For Au, Ti, and Pt, the Fermi pinning level for *n*–GaN is about 0.5-eV higher in the gap than for *p*–GaN. However, the pair of pinning positions are not at the same place within the band gap for each metal. For Ni, Pd, and Al, the pinning positions for *n*–GaN and *p*–GaN are very close or nearly identical within the band gap. The Fermi level pinning position may shift higher or lower for the specific metal.

The intensity of the Ga 3*d* core level from the substrate will be decreased by the presence of the metal overlayer. The intensity of the Ga 3*d* core level before (I_o) and after each deposition (I_s) is used to create a ratio I_s/I_o. The dependence of this ratio on the thickness of the metal deposited describes the growth mode of the metal on the GaN surface. The three modes of growth considered in this study are: Frank–van der Merwe (FM), Volmer–Weber (VW), and

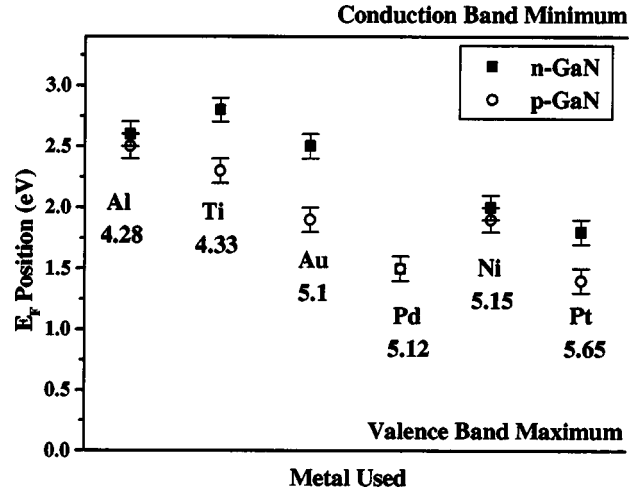

FIG. 6. A summary of the Fermi-level positions at the thick coverage extreme, for both *n*–GaN and *p*–GaN is given for various metals to illustrate the two types of Fermi-level pinning.

TABLE I. The Fermi level position within the 3.4-eV band gap of GaN in the limit of thick metal overlayers. The surface barrier heights (Φ_B) in electron volts are given for each metal deposited on both *n*–GaN and *p*–GaN. The literature values for the work function (Φ_m) in electron volts and electronegativity (χ_m) for each metal are also shown.

Metal deposited	Φ_m (eV)	χ_m (eV)	*n*–GaN, position of E_F with respect to VBM (eV)	*n*–GaN, $\Phi_{B,n}$ (eV)	*p*–GaN, position of E_F with respect to VBM, $\Phi_{B,p}$ (eV)
Al	4.28	1.61	2.6±0.1	0.8±0.1	2.5±0.1
Ti	4.33	1.54	2.8×0.1	0.6±0.1	2.3±0.1
Au	5.1	2.54	2.5±0.1	0.9±0.1	1.9±0.1
Pd	5.12	2.20	1.5±0.1	1.9±0.1	1.5±0.1
Ni	5.15	1.91	2.0±0.1	1.4±0.1	1.9±0.1
Pt	5.65	2.28	1.8±0.1	1.6±0.1	1.4±0.1

Stranski–Krastanov (SK).[30,31] These growth modes will exhibit different dependencies on surface metal coverage[32]

$$\text{Frank–van der Merwe Growth} \quad \frac{I_s}{I_o} = e^{(-\tau/\lambda)}, \tag{3}$$

$$\text{Volmer–Weber Growth} \quad \frac{I_s}{I_o} = (1-\theta) + \theta e^{(-t/\lambda)}, \tag{4}$$

$$\text{Stranski–Krastanov Growth} \quad \frac{I_s}{I_o} = (1-\theta)e^{(-q/t)} + \theta e^{(-t/\lambda)}, \tag{5}$$

where t is the film thickness and λ is the attenuation length of the electrons, both in nanometers, θ represents the fractional surface coverage reached prior to the island growth in three dimensions, and q is the thickness of the growing film that occurs via layer-by-layer growth before the islanding begins.[33,34] The attenuation length of the electrons is calculated from the thickness of a monolayer of the growing material and the kinetic energy of the substrate core level electron.[35,36] For Pt, the monolayer thickness was approximated by 0.25 nm. When using a photon energy of 75 eV, the kinetic energy of a photoemitted Ga 3*d* core-level electron will be 49.5 eV. An electron with this kinetic energy will have an attenuation length of 0.35 nm when passing through a Pt overlayer. A plot of the observed I_s/I_o ratio for deposition of Pt on both *n*–GaN and *p*–GaN substrates is shown in Fig. 7 along with the relationship calculated for each of the three growth modes.

Tapping mode AFM images were collected from the samples upon removal from the UHV chamber. AFM images from the bare *n*–GaN surface and the Au- and Ni-deposited samples are shown in Fig. 8.

DISCUSSION

Figure 7 indicates that Pt is not growing in a layer–by–layer (FM) fashion since the intensity ratio does not asymptotically approach zero. The growth behavior may be following either the VW or SK growth. The plots for the photoemission intensity ratio as a function of overlayer thickness for the other 5 metals indicate the lack of FM growth and the existence of VW or SK growth.

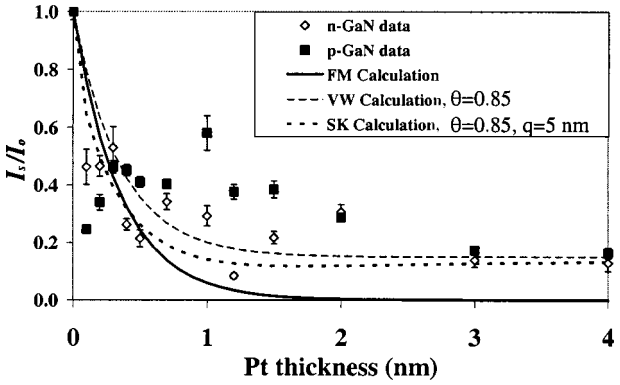

FIG. 7. The intensity of the Ga 3*d* core level before (I_o) and after each deposition (I_s) is used to create a ratio I_s/I_o. The intensity ratio, I_s/I_o, is plotted as a function of film thickness for the deposition of Pt metal on both *n*–GaN and *p*–GaN. The expected ratio as a function of thickness is plotted for each of the three growth modes: Frank–van der Merwe, Volmer–Weber, and Stranski–Krastanov growth.

From the AFM results, the Au is clearly forming islands with a size of approximately 50–60 nm in diameter and about 6–9 nm in height [Fig. 8(b)]. The AFM image of the Ni-deposited sample appears smooth, indicating that if islands are formed they are smaller than the resolution of the AFM measurement (~10 nm) or they have grown and coalesced [Fig. 8(c)]. The root-mean-squared (rms) roughness was determined from the 2×2 μm^2 AFM images. The rms roughness on the bare *n*–GaN was ~0.78 nm. With a 10-nm Au layer, the rms roughness was increased to ~1.87 nm and a 10-nm Ni layer possesses a value of ~0.76 nm. The AFM results for deposition of Ti, Al, Pd, and Pt on *n*–GaN are similar to what is shown for the Ni sample for both *p*– and *n*–GaN. The Au is clearly forming islands in the image. The other five metals could possibly be forming islands, but they are not observed as illustrated for Ni on *n*–GaN. Although there have been reports of layer–by–layer growth in the literature for Pd,[34] Pt,[37] and Au,[38] there has also been evidence for island formation. Island formation was observed via AFM for Pd, Au, and Al grown at room temperature.[38,39]

The surface-barrier height values determined in this study are similar to values found in the literature for related systems (Table II). When possible, these values are reported in the table for the specific combination of sample doping, chemical pretreatment, metal, and surface-barrier height measurement technique, closest to those used here.

The Schottky–Mott relationship predicts that, for *n*–type semiconductors, when $\Phi_m > \Phi_s$, the contact is rectifying; but when $\Phi_m < \Phi_s$, the contact is ohmic. For *p*–type semiconductors, the contact is ohmic when $\Phi_m > \Phi_s$, and the contact is rectifying for $\Phi_m < \Phi_s$. For GaN with $n \sim 2\times10^{17}$ cm^{-3}, the work function Φ_s is reported to be 4.2 ± 0.2 eV.[40] The value has been calculated via photoemission experiments on a biased sample according to Eq. (6)

$$\Phi = E_{\text{th}} + \Phi_{\text{CMA}} + eV_b \tag{6}$$

where V_b is the applied bias, E_{th} is the kinetic energy of the slow secondary electron threshold, and Φ_{CMA} is the work function of the CMA detector.[40] According to this value, all the metals studied should form a rectifying contact on *n*–GaN and an ohmic contact on *p*–GaN, since all of our metals have $\Phi_m > \Phi_s$. The Schottky–Mott theory also predicts, for *n*–type semiconductors with Φ_s less than Φ_m, that the surface-barrier height is equal to the difference between the work function of the contact metal Φ_m and the electron affinity χ_s of the semiconductor sample, given by Eq. (7).[41]

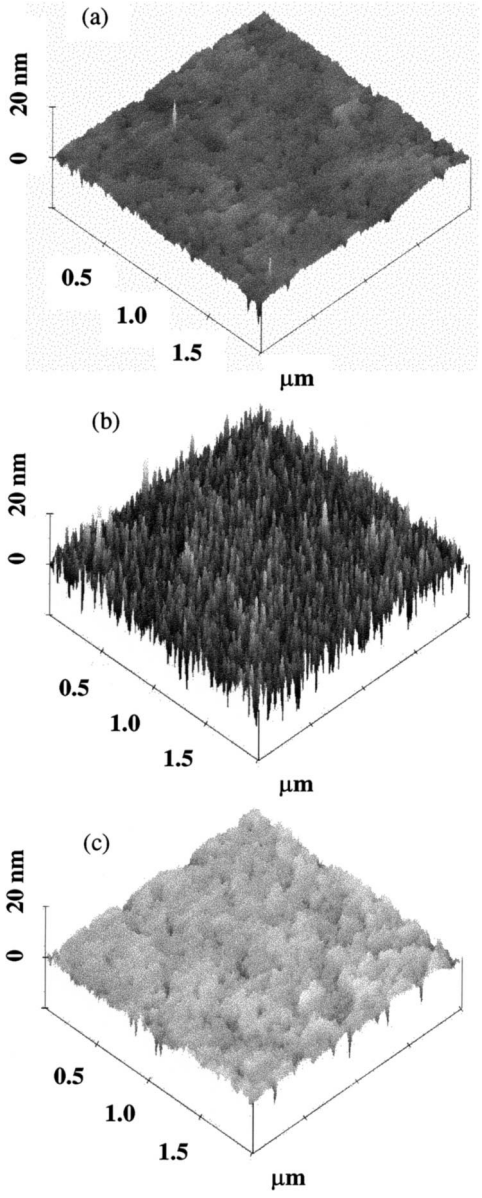

FIG. 8. The atomic force microscope images of a 2×2-μm^2 area of the sample surface of (a) the bare *n*–GaN surface (rms roughness of ~0.78 nm); (b) *n*–GaN with 10-nm-thick Au overlayer (rms roughness of ~1.87 nm); and (c) *n*–GaN with 10-nm-thick Ni overlayer (rms roughness of ~0.85 nm).

$$\Phi_{B,n} = \Phi_m - \chi_s. \tag{7}$$

Also, within the Schottky–Mott model the barriers to *n*–GaN ($\Phi_{B,n}$) and *p*–GaN ($\Phi_{B,p}$) for a given metal should sum to the band gap[42]

$$\Phi_{B,n} + \Phi_{B,p} = E_{\text{gap}} \tag{8}$$

and hence

$$\Phi_{B,p} = E_{\text{gap}} - (\Phi_m - \chi_s). \tag{9}$$

TABLE II. Surface-barrier heights measured for metals on GaN, using a variety of measurement techniques, for comparison to the results reported here.

Metal deposited	n–GaN, $\Phi_{B,n}$ (eV)	p–GaN, $\Phi_{B,p}$ (eV)
Al	0.6, 0.8,[a]	all ohmic
Ti	0.45,[b] 0.475,[c] 0.450[d]	0.65[e]
Au	0.9,[f] 0.96±0.2[g]	2.48[h]
Pd	0.94, 1.07, 0.92[i]	0.51[j]
Ni	1.13[k]	2.4±0.2[l]
Pt	1.57, 1.52, 1.6[m]	0.5[e]

[a]Reference 54.
[b]Reference 55.
[c]Reference 56.
[d]Reference 57.
[e]Reference 58.
[f]Reference 59.
[g]Reference 60.
[h]Reference 61.
[i]Reference 62.
[j]Reference 63.
[k]Reference 64.
[l]Reference 65.
[m]Reference 13.

As expected, for the metals that exhibit a single pinning position, Ni, Al, and Pd, the sum of the $\Phi_{B,n}$ and $\Phi_{B,p}$ values shown in Table I, is very close to the GaN band gap. In this respect, Ni, Al, and Pd, could be considered to follow Schottky–Mott-like behavior. For GaN, $\chi_s = 4.14$ has been reported.[43] Our results do show a deviation from the Φ_B values predicted by the Schottky–Mott theory using the above value for electron affinity. The Schottky–Mott theory also predicts a linear dependence of the surface-barrier height on the work function of the metal used in the contact with a slope of unity. While perfect Schottky–Mott behavior is not observed, the dependence of barrier height on the work function can still be described by a linear relationship. The slope parameter S is defined as follows:

$$S = \frac{\Delta\Phi_B}{\Delta\Phi_m} \leqslant 1. \tag{10}$$

The results of this study are plotted as a function of the metal work function in Fig. 9, and yield a roughly linear trend. For n–GaN [Fig. 9(a)], a slope of $\sim +0.7$ is observed. Previous reports for n–GaN show slopes of 0.43 and 0.81,[44] for analysis of photoemission-acquired barrier heights with samples with different premetallization preparations; and 0.385,[12] for plasma-treated samples with surface-barrier heights acquired with I-V curves. Also, a slope of 0.97 has been reported for I-V and CV measurements on KOH-treated n–GaN grown on SiC.[44,45] For p–GaN [Fig. 9(b)], a slope with a value of ~ -0.8 was observed. Koide *et al.* also reported a slope of -0.6 for p–GaN samples treated with a buffered hydrofluoric acid (HF) solution prior to metal deposition, with the surface-barrier height being calculated from I-V measurements.[46] Our results are in general agreement with these previous studies.

The Schottky–Mott model assumes that there is no interfacial layer between the metal and the semiconductor and that there are no surface states on the semiconductor. For example, GaAs does not follow the prediction of the Schottky–Mott rule as shown in the literature compilation of measured surface-barrier heights[42] and this deviation is attributed to electronic states at the metal-semiconductor interface. A variety of models have been proposed that include

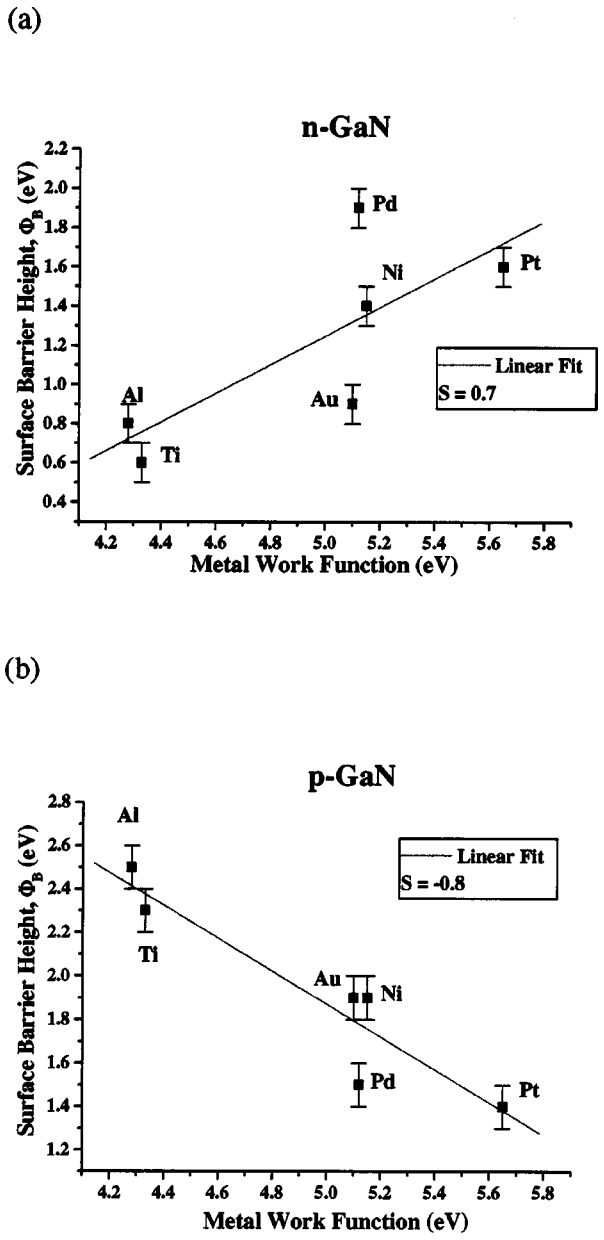

FIG. 9. The measured surface-barrier heights are shown as a function of the work function of the metal used for the contact formation. Results for (a) n–GaN and (b) p–GaN. S is the slope of a linear fit.

interface or surface electronic states in a model of the Schottky barrier formation. The virtual gap states model assumes that a continuum of gap states exists in the band gap, as calculated from Schrödinger's equation for complex wave vectors present at the semiconductor surface.[42] Heine proposed the MIGS (metal-induced gap states) model, which leads to a linear relationship between the barrier heights and the electronegativity difference between the semiconductor and the metal.[42] There is, however, no such apparent trend of the results from this study with the electronegativity difference between the semiconductor (GaN electronegativity, $\Delta\chi = 1.23$) and the metal χ_m (listed in Table I.). Spicer *et al.* proposed the unified defect model, in which the deposition of metal atoms creates defects on the semiconductor surface that give rise to donorlike and acceptorlike states.[47–49] This

mechanism would lead to a separate pinning position for *n*– and *p*–GaN, as observed for Au, Ti, and Pt overlayers. This is consistent with our choice of chemical treatments for the samples prior to metallization. For *n*–GaN, HCl has been shown previously to decrease the surface-barrier height presumably through creation of N vacancies that pin E_F close to the conduction-band minimum (CBM).[4] For aqua regia treatment of *p*–GaN, it has been shown that E_F pins near the valence-band maximum (VBM), coincident with the Ga vacancy states, decreasing the surface-barrier height.[7]

Al and Ti may be expected to behave similarly, since both are strong nitride formers (AlN and TiN). Al may also form AlGaN, which could act as an interfacial layer with an increased band gap. Ti may also form several gallides, while Al will not.[50,51] With Ti, it is also possible that the ternary phase Ti_2GaN could form as an interfacial layer.[52] Previous literature calculations do predict the presence of MIGS for the deposition of Al on GaN that tail into the semiconductor so that the first few layers of the semiconductor have metallic character.[53] However, the Fermi-level pinning behavior for Al and Ti is different: Al exhibits a single pinning energy within the band gap for both *n*- and *p*-type GaN, while Ti shows a 0.5 eV difference between the *n*–GaN and *p*–GaN.

CONCLUSIONS

Two Fermi-level pinning behaviors are seen over the range of metals investigated. Specific chemical surface treatments were used for the predeposition preparation of the *n*– and *p*–GaN. For Ti, Au, and Pt, two pinning positions are observed within the band gap depending on the carrier type, perhaps indicating the presence of two types of surface states created by the predeposition chemical treatments. For the three other metals, Ni, Al, and Pd, a single pinning position was observed for *n*– and *p*–GaN. The barrier heights for Ni, Pd, and Al exhibit a modified Schottky-Mott behavior, while the results for Au, Ti, and Pt demonstrate a more complex behavior.

ACKNOWLEDGMENTS

The authors would like to thank Samsung Advanced Institute of Materials for supplying the *p*–GaN samples, Ling Zhang for supplying the *n*–GaN, and Chris Pelto and Professor Austin Chang at the UW-Madison for helpful discussions and facility use. J. K. Kim and J.-L. Lee would like to thank the project ''National Research Laboratory'' sponsored by the Korea Institute of Science and Technology Evaluation and Planning (KISTEP). This work is supported by the National Science Foundation. Research and facility support through the UW-Madison's Materials Research Science and Engineering Center (MRSEC) on Nanostructured Materials and Interfaces and the Synchrotron Radiation Center at the UW-Madison (DMR-0084402) is gratefully acknowledged.

[1] S. Nakamura, MRS Bull. **22**, 29 (1997).
[2] S. Nakamura, *The Blue Laser Diode: The Complete Story* (Springer, Berlin, 2000).
[3] J. Sun, K. A. Rickert, J. M. Redwing, A. B. Ellis, F. J. Himpsel, and T. F. Kuech, Appl. Phys. Lett. **76**, 415 (2000).
[4] K. A. Rickert, J. Sun, A. B. Ellis, F. J. Himpsel, and T. F. Kuech, Appl. Phys. Lett. **80**, 204–206 (2002).
[5] J.-L. Lee, J. K. Kim, J. W. Lee, Y. J. Park, and T. Kim, Phys. Status Solidi A **176**, 763 (1999).
[6] J. K. Kim, J.-L. Lee, J. W. Lee, Y. J. Park, and T. Kim, J. Vac. Sci. Technol. B **17**, 497 (1999).
[7] J. K. Kim, K.-J. Kim, B. Kim, J. N. Kim, J. S. Kwak, Y. J. Park, and J.-L. Lee, J. Electron. Mater. **30**, 129 (2001).
[8] K. Suzue, S. N. Mohammad, Z. F. Fan, W. Kim, O. Aktas, A. E. Botchkarev, and H. Morkoç, J. Appl. Phys. **80**, 4467 (1996).
[9] E. Kaminska, A. Piotrowska, M. Guziewicz, S. Kasjaniuk, A. Barcz, E. Dynowska, M. D. Bremser, O. H. Nam, and R. F. Davis, Mater. Res. Soc. Symp. Proc. **449**, 1055 (1997).
[10] S. C. Binari, H. B. Dietrich, G. Kelner, L. B. Rowland, K. Doverspike, and D. K. Gaskill, Electron. Lett. **30**, 909 (1994).
[11] E. C. Piquette, Z. Z. Bandic, and T. C. McGill, Mater. Res. Soc. Symp. Proc. **482**, 1089 (1998).
[12] A. C. Schmitz, A. T. Ping, M. Asif Khan, Q. Chen, J. W. Yang, and I. Adesida, J. Electron. Mater. **27**, 255 (1998).
[13] J. M. DeLucca, S. E. Mohney, F. D. Auret, and S. A. Goodman, J. Appl. Phys. **88**, 2593 (2000).
[14] D. Qiao, L. S. Yu, S. S. Lau, J. Y. Lin, H. X. Jiang, and T. E. Haynes, J. Appl. Phys. **88**, 4196 (2000).
[15] D. Mistele, F. Fedler, H. Klausing, T. Rotter, J. Stemmer, O. K. Semchinova, and J. Aderhold, J. Cryst. Growth **230**, 564 (2001).
[16] J. S. Kwak, S. E. Mohney, J.-Y. Lin, and R. S. Kern, Semicond. Sci. Technol. **15**, 756 (2000).
[17] D. J. King, L. Zhang, J. C. Ramer, S. D. Hersee, and L. F. Lester, Mater. Res. Soc. Symp. Proc. **468**, 421 (1997).
[18] L.-C. Chen, J.-K. Ho, C.-S. Jong, C. C. Chiu, K.-K. Shih, F.-R. Chen, J.-J. Kai, and L. Chang, Appl. Phys. Lett. **76**, 3703 (2000).
[19] T. Kim, M. C. Yoo, and T. Kim, Mater. Res. Soc. Symp. Proc. **449**, 1061 (1997).
[20] J.-S. Jang, I.-S. Chang, H.-K. Kim, T.-Y. Seong, S. Lee, and S.-J. Park, Appl. Phys. Lett. **74**, 70 (1999).
[21] S. Ruvimov, Z. Liliental-Weber, J. Washburn, K. J. Duxstad, E. E. Haller, Z.-F. Fan, S. N. Mohammad, W. Kim, A. E. Botchkarev, and H. Morkoç, Appl. Phys. Lett. **69**, 1556 (1996).
[22] S. Hüfner, *Photoelectron Spectroscopy*, 2nd ed. (Springer-Verlag, Berlin, 1996), Vol. 82.
[23] D. K. Schroder, *Semiconductor Material and Device Characterization* (Wiley, New York, 1990).
[24] R. T. Tung, Mater. Sci. Rep. **R35**, 1 (2001).
[25] F. J. Himpsel, Surf. Sci. Rep. **12**, 1 (1990).
[26] A. Barinov, L. Casalis, L. Gregoratti, and M. Kiskinova, Phys. Rev. B **63**, 085 308(1–6) (2001).
[27] A. Barinov, L. Casalis, L. Gregoratti, and M. Kiskinova, J. Phys. D **34**, 279 (2001).
[28] M. Alonso, R. Cimino, and K. Horn, Phys. Rev. Lett. **64**, 1947 (1990).
[29] K. A. Rickert, J. K. Kim, J.-L. Lee, F. J. Himpsel, A. B. Ellis, and T. F. Kuech, Mater. Res. Soc. Symp. Proc. **693**, I13.4.1 (2002).
[30] J. A. Venables, *Introduction to Surface and Thin Film Processes* (Cambridge University, Cambridge, 2000).
[31] J. A. Venables, Surf. Sci. **299/300**, 798 (1994).
[32] P. H. Holloway, J. Vac. Sci. Technol. **12**, 1418 (1975).
[33] Z. Sitar, L. L. Smith, and R. F. Davis, J. Cryst. Growth **141**, 11 (1994).
[34] P. J. Hartlieb, A. Roskowski, R. F. Davis, W. Platow, and R. J. Nemanich, J. Appl. Phys. **91**, 732 (2002).
[35] D. Briggs and M. P. Seah, *Practical Surface Analysis*, Vol. 1: Auger and X-ray Photoelectron Spectroscopy, 2nd ed. (Wiley, Guildeford, Surrey, 1990).
[36] M. P. Seah and W. A. Dench, Surf. Interface Anal. **1**, 2 (1979).
[37] E. A. Preble, K. M. Tracy, S. Kiesel, H. McLean, P. Q. Miragila, R. J. Nemanich, R. F. Davis, M. Albrecht, and D. J. Smith, J. Appl. Phys. **91**, 2133 (2002).
[38] R. Sporken, C. Silien, F. Malengreau, K. Grigorov, R. Caudano, F. J. Sánchez, E. Calleja, E. Muñoz, B. Beaumont, and P. Gibart, MRS Internet J. Nitride Semicond. Res. **2**, 23 (1997).
[39] Q. Z. Liu, K. V. Smith, E. T. Yu, S. S. Lau, N. R. Perkins, and T. F. Kuech, Mater. Res. Soc. Symp. Proc. **449**, 1079 (1997).
[40] V. M. Bermudez, T. M. Jung, K. Doverspike, and A. E. Wickenden, J. Appl. Phys. **79**, 110 (1996).
[41] E. H. Rhoderick and R. H. Williams, *Metal-Semiconductor Contacts*, 2nd ed. (Oxford University, Oxford, 1988), Vol. 19.

[42] W. Mönch, *Semiconductor Surfaces and Interfaces*, 2nd ed. (Springer, Berlin, 1993), Vol. 26.
[43] S. Miller and P. H. Holloway, J. Electron. Mater. **25**, 1709 (1996).
[44] V. M. Bermudez, J. Appl. Phys. **86**, 1170 (1999).
[45] E. V. Kalinina, N. I. Kuznetsov, V. A. Dmitriev, K. G. Irvine, and C. H. Carter, Jr., J. Electron. Mater. **25**, 831 (1996).
[46] Y. Koide, H. Ishikawa, S. Kobayashi, S. Yamasaki, S. Nagai, J. Umezaki, M. Koike, and M. Murakami, Appl. Surf. Sci. **117/118**, 373 (1997).
[47] W. E. Spicer, P. W. Chye, P. R. Skeath, C. Y. Su, and I. Lindau, J. Vac. Sci. Technol. **16**, 1422 (1979).
[48] W. E. Spicer, Z. Liliental-Weber, E. Weber, N. Newman, T. Kendelewicz, R. Cao, C. McCants, P. Mahowald, K. Miyano, and I. Lindau, J. Vac. Sci. Technol. B **6**, 1245 (1988).
[49] W. E. Spicer, I. Lindau, P. Skeath, and C. Y. Su, J. Vac. Sci. Technol. **17**, 1019 (1980).
[50] *Binary Alloy Phase Diagrams*, 2nd ed. (ASM International, Materials Park, OH, 1990), Vols. 1 and 2.
[51] F. R. de Boer, R. Boom, W. C. M. Mattens, A. R. Miedema, and A. K. Niessen, *Cohesion In Metals-Transition Metal Alloys* (North-Holland, Amsterdam, 1988).
[52] S. E. Mohney and X. Lin, J. Electron. Mater. **25**, 811 (1996).
[53] S. Picozzi, A. Continenza, S. Massidda, A. J. Freeman, and N. Newman, Phys. Rev. B **58**, 7906 (1998).
[54] C. I. Wu, A. Khan, A. E. Wickenden, D. Koleske, and R. L. Henry, J. Appl. Phys. **89**, 425 (2001).
[55] M. T. Hirsch, K. J. Duxstad, and E. E. Haller, Electron. Lett. **33**, 95 (1997).
[56] M. T. Hirsch, K. J. Duxstad, and E. E. Haller, Mater. Res. Soc. Symp. Proc. **449**, 1115 (1997).
[57] M. T. Hirsch, K. J. Duxstad, E. E. Haller, S. Ruvimov, and Z. Liliental-Weber, J. Electron. Mater. **27**, 1236 (1998).
[58] T. Mori, T. Kozawa, T. Ohwaki, Y. Taga, S. Nagai, S. Yamasaki, S. Asami, N. Shibata, and M. Koike, Appl. Phys. Lett. **69**, 3537 (1996).
[59] W. Liu, M.-F. Li, S.-J. Chua, N. Akutsu, and K. Matsumoto, J. Electron. Mater. **28**, 360 (1999).
[60] F. D. Auret, S. A. Goodman, F. K. Koschnick, J.-M. Spaeth, B. Beaumont, and P. Gibart, MRS Internet J. Nitride Semicond. Res. **4S1**, G6.13 (1999).
[61] N. I. Kuznetsov, E. V. Kalinina, V. A. Soloviev, and V. A. Dmitriev, Mater. Res. Soc. Symp. Proc. **395**, 837 (1996).
[62] A. T. Ping, A. C. Schmitz, M. Asif Khan, and I. Adesida, Electron. Lett. **32**, 68 (1996).
[63] J.-L. Lee and J. K. Kim, J. Electrochem. Soc. **147**, 2297 (2000).
[64] A. C. Schmitz, A. T. Ping, M. Asif Khan, and I. Adesida, Mater. Res. Soc. Symp. Proc. **395**, 831–835 (1996).
[65] K. Shiojima, T. Sugahara, and S. Sakai, Appl. Phys. Lett. **74**, 1936 (1999).